MPI-PhE/99-03

Latest Highlights from the H1 Collaboration

Tancredi Carli[a*]

[a]Max-Planck Institut für Physik,
Föhringer Ring 6, 80805 München

Recent data obtained in e^+p collisions at HERA by the H1 collaboration are presented: searches for new phenomena beyond the Standard Model, measurement of the inclusive neutral and charged current cross sections and of the proton structure function, determination of the gluon density in the proton and photon from jet productions, measurement and interpretation of event shapes in the current region of the Breit frame, test of the parton evolution at low x and of the diffractive production mechanism.

1. Introduction

The electron-proton collider HERA offers the unique possibility to explore the complex structure of the proton in a relatively clean environment. The large centre of mass energy of $\sqrt{s} \approx 300$ GeV allows a perturbative QCD analysis in a previously inaccessible domain. Compared to fixed target experiments HERA extends the kinematic reach of deep-inelastic scattering (DIS) by about of two orders of magnitude in the Bjorken variable x and the photon virtuality Q^2. The understanding of the proton structure is in many aspects a challenge to theory and therefore interesting in itself. Furthermore, the proton is the particle which gives access to the highest possible centre of mass energy in particle collisions. The knowledge of the (non-perturbative) parton density function in the proton and the theoretical understanding how they evolve in the different kinematic regimes is therefore an important prerequisite for any possible future discovery of new phenomena, e.g. in proton proton collisions at LHC.

Within the Standard Model many aspects of the strong interactions remain unexplained. HERA has here the peerless opportunity to link QCD to the general analytic properties of the scattering amplitudes as e.g. exploited in the Regge phenomenology. Such theories have been very sucessful to describe elastic and diffractive scattering at high energies and the energy dependences of the total hadronic cross section. First steps to understand the dynamics of the transformation of a complex coloured system in a colour singlet probed by a virtual photon have been very sucessful.

In the period 1994−1997 HERA colliding $E_e = 27.5$ GeV positrons on $E_p = 820$ GeV protons has delivered an integrated luminosity of about $\int \mathcal{L}\, dt = 37$ pb^{-1} of useful data to H1. Most of the results in this report will be based on this data set. Since 1998 HERA has switched back to electrons and about $\int \mathcal{L}\, dt = 15$ pb^{-1} have been collected. First results based on $\int \mathcal{L}\, dt = 5.6$ pb^{-1} from electron-proton collisions are already available. This represents an increase in e^-p data by a factor of 10. In addition the proton energy was pushed to $E_p = 920$ GeV leading to a higher centre of mass energy and to a higher parton luminosity at fixed x.

2. Search for New Phenomena at Highest Energy

The high momentum transfers accessible at HERA allow the proton to be probed at very small distances down to 10^{-16} cm via exchange of highly virtual gauge bosons. Particles with masses higher than the centre of mass energy could be exchanged in the t-channel. Their interference with standard DIS processes could be experimentally observed as enhancement or deficit in the NC cross section at high Q^2 or at high mass. Moreover, new particles with masses up

*Invited plenary talk at VII. Int. workshop on DIS and QCD, April 1999, Zeuthen-Berlin

to 300 GeV could be produced as s-channel resonances. HERA is here particularly sensitive to particles coupling to electrons and quarks in the proton.

2.1. Inclusive Searches

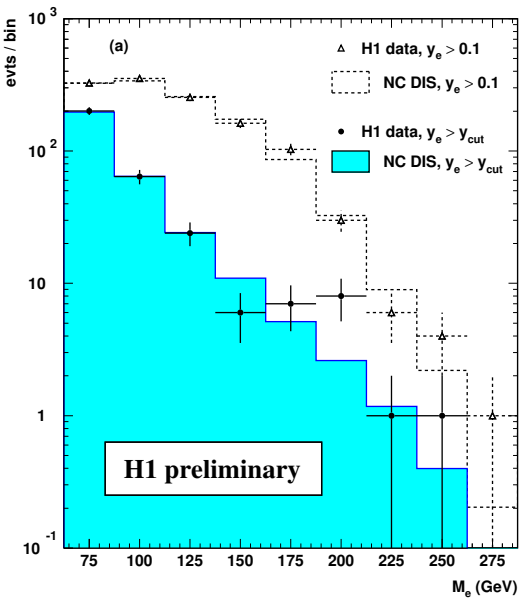

Figure 1. *$M = \sqrt{sx}$ distribution for the inclusive $e^+p \to e^+X$ sample and for a optimised cut in y. Shown are H1 data and the DIS expectation.*

In an analysis of the data taken in 1994 to 1996 an excess of neutral current data $e^+p \to e^+X$ at very high Q^2 has been found. 12 events with $Q^2 > 15000$ GeV^2 have been observed in the data while only 4.71 ± 0.76 were expected by standard DIS. 7 of these events had an invariant mass $M = \sqrt{sx}$ in a window of 25 GeV around $M = 200$ GeV and $y > 0.4$. In 1997 the total luminosity was doubled. Also in this data a tendency for more events at high Q^2 has been found. The magnitude of the excess is however not confirmed. Above $Q^2 > 15000$ GeV^2 22 events are found and 14.7 ± 2.1 are expected. 8 events fall in the mass window at $M = 200$ GeV and 3.01 ± 0.54 are expected.

The mass distribution of all e^+p data is shown in Fig. 1. The standard DIS background is known within $\pm 5 - 10\%$. If the new particle has spin 0, the angular distribution of the decay product is flat. The $y = 1/2\,(1 + \cos\theta^*)$ distribution[2] will therefore be flat, as opposed to DIS where the cross section falls like $1/y^2$. The signal to background ratio can therefore be optimised by a cut in y. The mass distribution for a $y_{cut}(M)$ optimised for each mass bin, is also shown in Fig. 1. From this mass spectrum upper limits on scalar and vector leptoquarks classified according to their spin, weak isospin and fermion number [1] have been derived. If the strength of this new e^+q coupling is the same as for the electromagnetic coupling, than masses up to 275 GeV are excluded. If one allows for a branching $LQ \to eq$ of e.g. 10%, masses up to 255 GeV are ruled out by the data. For these small branchings this limit extents far beyond the domain presently covered in $p\bar{p}$ collisions.This has triggered intensive searches for other signatures.No signal has been found in the reactions $e^\pm p \to \mu^\pm p$ and $e^\pm p \to \tau^\pm p$. However, the derived limits on leptoquarks decaying in the second or third generation are better as or competitive with low energy experiments in most cases [2].

2.2. Muon Events

In an inclusive search for events with a high transverse momentum of the hadronic final state above 25 GeV, six events with high energetic isolated leptons ($P_T^\star > 10$ GeV) have been observed. One event has an electron and five have a muon in the final state. In all events an imbalance of missing longitudinal and transverse momentum is measured suggesting the presence of an undetectable particle like a neutrino. The electron event and two muon events are found in the phase space where the most important background - the direct production of W bosons $ep \to WX$ - are expected. In the muon (electron) channel 0.8 ± 0.2 (2.4 ± 0.5) events are expected and 5 (1) have been observed.

The striking characteristics of the muon events is the large amount of transverse energy of the hadronic system (P_T^X) which is displayed together with lepton-neutrino transverse mass ($M_T^{\mu\nu}$) in Fig. 2. Overlayed is the expected distribution of direct production of W bosons. It would be how-

[2] θ^* is the lepton-parton angle in the centre of mass system of the decaying particle.

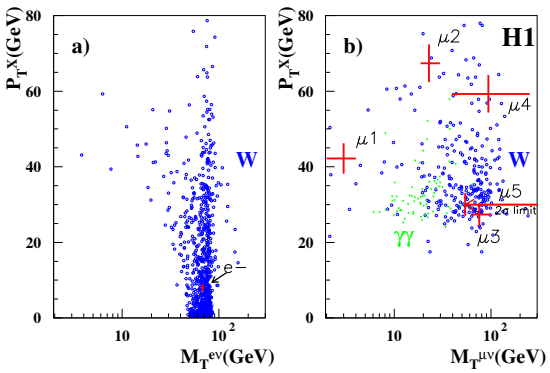

Figure 2. *Transverse momentum of the hadronic final state as a function of the transverse mass of the lepton-neutrino system for events with isolated leptons. The crosses gives the* 1σ *uncertainty on the measured parameters. The expected distribution for direct* $W^{\pm}$ *production and muon production in* $\gamma\gamma$ *processes is overlayed.*

ever interesting to know how QCD effects which are presently not included in the background estimation using the event generator EPVEC [3], could alter the P_T^X and $M_T^{\mu\nu}$ distribution. In the 1998/1999 e^-p data no events with isolated leptons have been found. For a luminosity of $\int \mathcal{L}\, dt = 5.1$ pb^{-1} 0.14 ± 0.04 (0.37 ± 0.07) events are expected in the muon (electron) channel.

3. Inclusive Neutral and Charged Current Single Differential Cross Sections

3.1. Neutral Current Events

The Standard Model neutral current cross section can be represented in the form:

$$\frac{d^2\sigma^{e^{\pm}p}}{dxdQ^2} = \frac{2\pi\alpha^2}{xQ^4}\left[Y_+\tilde{F}_2(x,Q^2) - y^2 F_L(x,Q^2) \mp Y_- xF_3(x,Q^2)\right]$$

where α is the electromagnetic coupling constant and $Y_{\pm} = 1 \pm (1-y)^2$ contains the helicity dependence of the electroweak interaction.

The generalised proton structure function $\tilde{F}_2(x,Q^2)$ can be decomposed in:

$$\tilde{F}_2 = F_2^{em} + \frac{Q^2}{Q^2+M_Z^2}F_2^{\gamma Z} + \left(\frac{Q^2}{Q^2+M_Z^2}\right)^2 F_2^Z$$

where F_2^{em} describes the pure photon exchange, $F_2^{\gamma Z}$ the γZ interference and F_2^Z the pure exchange of the Z boson. $\tilde{F}_2$ is sensitive to the singlet sum of the quark distributions $(xq + x\bar{q})$. xF_3

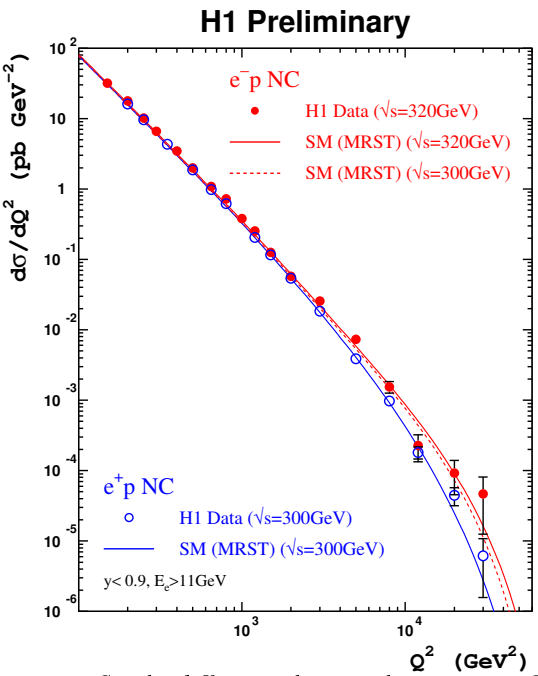

Figure 3. *Single differential neutral current DIS cross section as a function of* Q^2.

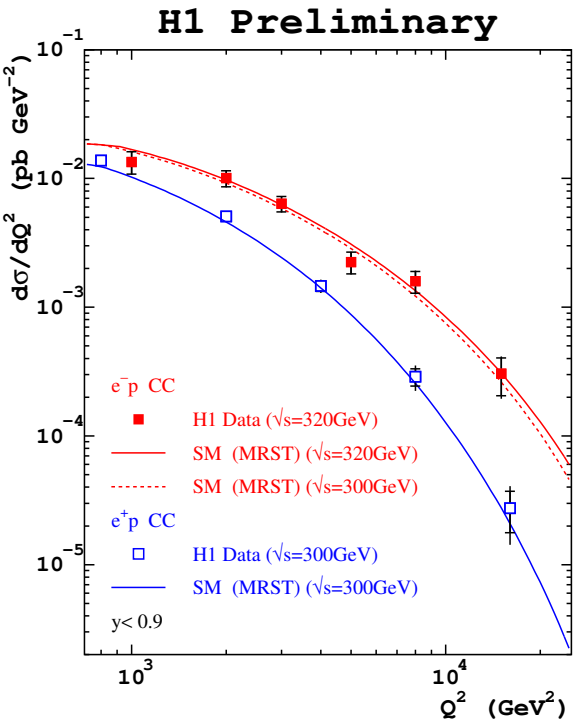

Figure 4. *Single differential charged current DIS cross section as a function of* Q^2.

is the parity violating proton structure function which is sensitive to the non-singlet difference of the quark densities $(xq - x\bar{q})$ and is given by:

$$F_3 = \frac{Q^2}{Q^2 + M_Z^2} F_3^{\gamma Z} + \left(\frac{Q^2}{Q^2 + M_Z^2} \right)^2 F_3^Z$$

F_3 contributes with different sign to the cross section for the e^- and e^+ case. Below $Q^2 \lesssim 1500$ GeV^2 contributions from Z exchange are smaller than 1%, but at high Q^2 the inclusive cross section is sensitive to electroweak effects (at $Q^2 = 5000$ GeV^2 and $x = 0.08$: $\delta_z - \delta_3 \approx 10\%$).

The longitudinal structure function F_L contributes less than 5% at very high y and is negligible below $y \leq 0.4$.

The single differential cross section is shown as a function of Q^2 in Fig. 3 for both e^+p and e^-p scattering. The e^-p data have been taken in 1998/1999 and correspond to the $\int \mathcal{L}dt \approx 5$ pb^{-1} analysed up to March 1999.

The cross section falls like $1/Q^4$ over 6 orders of magnitude and spans 2 orders of magnitude in Q^2. For $Q^2 > 3000$ GeV^2 the e^-p data are always above the e^+p data. This provides for the first time evidence for γZ interference effects in $e^\pm p$ scattering. The increase of the centre of mass energy from $\sqrt{s} = 300$ to 320 GeV does not influence this conclusion, since it leads only to a marginal increase of the cross section (see dashed line in Fig. 3). While in the e^-p case good agreement is found with the Standard Model expectation, in the e^+p case a slight overshoot is observed at the highest Q^2. The theoretical uncertainty mainly introduced by the parton density functions is about 7% at the highest accessible Q^2 values.

3.2. Charged Current Events

Charged current events are characterised by their missing transverse momentum due to the undetected neutrino in the final state. Their cross section is given by:

$$\frac{d^2\sigma_{CC}^{e^\pm p}}{dxdQ^2} = \frac{G_F^2}{2\pi x} \left(\frac{M_{prop}^2}{Q^2 + M_{prop}^2} \right)^2 \cdot x \cdot \Phi_{CC}^{e^\pm p}(x, Q^2)$$

where G_F is the Fermi constant and M_{prop} is the mass of the space like charged exchanged boson which is in the SM the W boson. In leading order the helicity weighted parton density function have the simple form:

$$\Phi_{CC}^{e^+p}(x, Q^2) = (\bar{u} + \bar{c}) + (1 - y)^2 \cdot (d + s + b)$$

$$\Phi_{CC}^{e^-p}(x, Q^2) = (u + c) + (1 - y)^2 \cdot (\bar{d} + \bar{s} + \bar{b})$$

The positrons (electrons) only interact with quarks or anti-quarks with negative (positive) electric charge. In the e^-p (e^+p) case mostly (anti-)quarks are involved in the interaction.

Fig. 4 shows the charged current cross section as a function of Q^2. The e^-p data are an order of magnitude above e^+p data. This is due to the fact that in the e^-p case the cross section is proportional to $(u + c)$ while for e^+p the coupling to valence quark is suppressed by $(1 - y)^2$ $(d + s)$. Moreover is the d quark density smaller than the u quark density in the proton.

The charged current cross section falls over four orders of magnitudes in Q^2. From the Q^2 dependence the propagator mass has been determined to be:

$$M_{prop} = 81.2 \pm 3.3\,(stat.) \pm 4.3\,(syst)\ \text{GeV}$$

This result is compatible with the world average of the time-like W mass $M_W = 80.41 \pm 0.1$ GeV [4].

At high Q^2 the charged current cross section is suppressed relative to the neutral current cross section due to the d/u ratio being less than unity. From this observation it has been determined that at $x = 0.3$ the u valence quark density is approximately $1.5 - 3$ times larger than d valence quark density. A determination of u/d ratio at large x free from uncertainties due to nuclear binding effects will be possible in the future.

These measurements represent a benchmark for the Standard Model of electroweak interactions. More e^-p and e^+p data at the highest possible Q^2 are needed to get the best sensitivity. HERA will increase the luminosity in the year 2000. High statistics data will then allow a better understanding of the detector and decisive tests for deviation from the standard model are possible. This physics is just starting at HERA and a surprise is possible!

4. Measurement of the Proton Structure Function

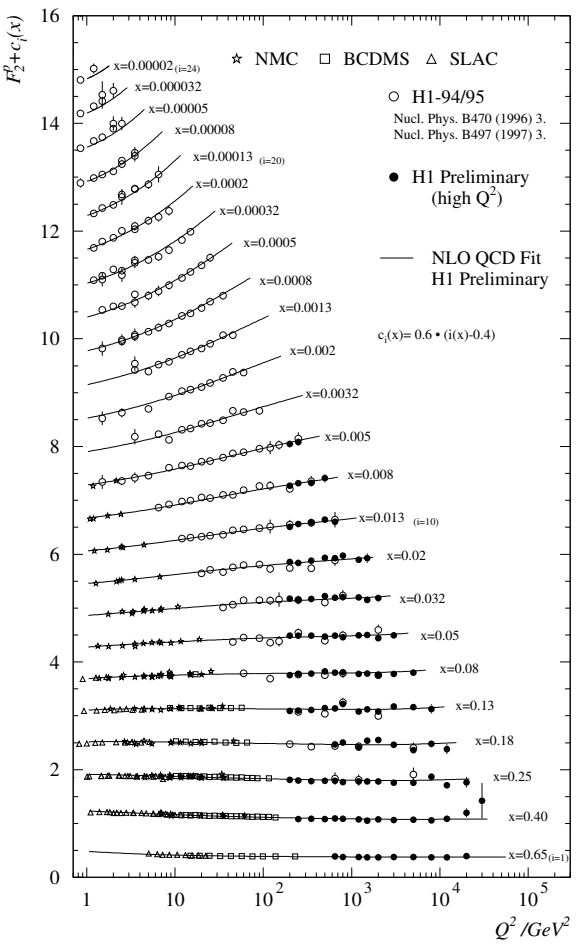

Figure 5. *The proton structure function F_2 as a function of Q^2 for bins in the Bjorken scaling variable x. Superimposed is a NLO QCD fit.*

A classic key measurement for the understanding of the proton structure is the precise determination of F_2 by counting inclusively the lepton scattered off the proton. The kinematic domain spans about 5 orders of magnitude in Q^2 from $1 \lesssim Q^2 \lesssim 30000$ GeV^2 and covers the momentum range from the sea quark region at low x ($x \gtrsim 2 \cdot 10^{-5}$) to the valence quark region at large x ($x \lesssim 0.65$).

An inclusive measurement has the advantage that it can be directly compared to QCD calculations. However, small interesting effects on top of the dominating parton evolution are difficult to reveal. Therefore F_2 has to be precisely pined down to get a handle on the QCD evolution and to constrain the non-perturbative parton density functions. A summary of the presently available data is shown in Fig. 5. For $x \leq 0.01$ the statistical error is about $\lesssim 1\%$ and the systematic accuracy has reached $\lesssim 3-4\%$ in most of the covered range. The largest experimental systematic errors are introduced by the hadronic and electromagnetic energy scale uncertainties.Compared to previous H1 results [5–7] the systematic uncertainties improved by nearly a factor of two. This precision can compete with the fixed target data.

The measurement extents to energies of the scattered positron down to 3 GeV. This was only possible by using the backward electromagnetic fibre-lead calorimeter SPACAL (operated since 1995) and by using the backward silicon strip detector (operated since 1997) to measure tracks within $172^o < \theta_{el} < 177^o$. It gives access to the kinematic region of low Q^2 and high $y \lesssim 0.75$ where the DIS cross section is sensitive to F_L. A new method has been introduced to improve the sensitivity to F_L by measuring the derivative:

$$\frac{\partial \sigma}{\partial \log y} = \frac{\partial F_2}{\partial \log x} - F_L \cdot \frac{2-y}{Y_+^2} + \frac{\partial F_L}{\partial \log x} \cdot \frac{y^2}{Y_+}$$

at fixed Q^2. Assuming that $\partial\sigma/\partial \log y$ is a linear function of $\log y$ up to large y, the contribution of F_2 at high y has been extrapolated by a straight line fit for $y < 0.2$. The extracted F_L extents down to $Q^2 = 3$ GeV at $x \approx 10^{-4}$ and is in good agreement with previous H1 results [8] and consistent with F_L as calculated by NLO QCD.

The NLO fit shown in Fig. 5 is performed in the $\overline{MS}$ renormalisation scheme using the NLO DGLAP evolution equations for three light flavours with the charm contribution added in the massive scheme according to a NLO calculation of the boson-gluon fusion process. The input distributions of the valence (u_v, d_v) and sea ($S = \bar{u} = \bar{d} = 2\bar{s}$) quarks and the gluon are parameterised at a starting scale $Q_0^2 = 2$ GeV^2 using 5 parameters which are determined in a fit to the data. The muon-proton data of BCDMS [9] and

the muon-deuteron data of NMC [10] are included in the fit to constrain the high x behaviour of the parton distributions. Target mass corrections were applied for the fixed target data. The strong coupling constant was set to $\alpha_s(M_Z^2) = 0.118$ and the charm quark mass to $m_c = 1.5$ GeV. This fit gives a good description of the data for all Q^2 and x. At low x the behaviour of F_2 is dominated by the gluon and the sea quark distributions. No need for a parton evolution different from NLO DGLAP is found.

5. Jet production in DIS

The high centre of mass energy of HERA leads to a large phase space for hadron production and to the possibility to observe clear jet structures in DIS. Jets are infrared and collinear safe observables defined by an algorithm relating the unobservables quarks and gluons to the sprays of hadrons observed in the detector. Events with two jets in the central part of the detector can be produced in quark ($q\gamma \to qg$) or gluon ($g\gamma \to q\bar{q}$) induced hard processes. The leading order Feynman diagrams for dijet production are shown in Fig. 6. Dijet cross sections are directly sensitive to the strong coupling constant α_s and to the gluon densities in the proton. They can be calculated in pQCD to NLO in α_s using numerical methods implemented in several Monte Carlo programs. In a frame[3], where the virtual photon γ and the proton p collide head-on, it is obvious that two scales can characterise the hardness of the process: Q^2 as used in the QCD analysis of the inclusive DIS cross section or the transverse momenta of the two jets E_T as used in hadron-hadron collisions.

H1 has reported the first fundamental understanding of jet production in DIS at HERA energies at the DIS 98 conference by demonstrating that dijet cross sections for $10 < Q^2 < 5000\,\mathrm{GeV}^2$ and $8.5 < E_T < 35$ GeV can be described by NLO QCD. Jets were defined by the inclusive K_T algorithm [11,12] in the Breit frame requiring two jets with $E_T > 5$ GeV and $E_{T,1} + E_{T,2} > 17$ GeV. Only jets lying well within the detector acceptance $-1 < \eta_{\mathrm{jet,lab}} < 2.5$ are considered.

[3] e.g. the hadronic centre of mass frame defined by $\vec{\gamma} + \vec{p} = 0$ or the Breit frame defined by $\vec{\gamma} + 2\,x\,\vec{p} = 0$.

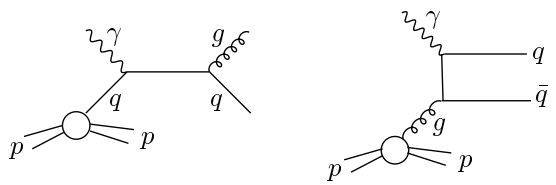

Figure 6. *Leading order feynman diagram for dijet production in DIS at HERA.*

At this conference further progress has been reported. The double differential single inclusive jet cross section $d\sigma/dQ^2dE_T$ for $7 < E_T < 50$ GeV has been made available. It is observed that for higher Q^2 the E_T spectrum gets harder. Moreover dijet rates $1/Ndn/dy_2$, where y_2 is the maximal value of the resolution parameter which allows to resolve two jets in an event, have been measured for $150 < Q^2 < 5000\,\mathrm{GeV}^2$ using the Durham K_T algorithm [13] with a scale of $100\ \mathrm{GeV}^2$. Also the y_2 spectrum gets harder as Q^2 increases, i.e. harder jet structures are resolved. Both observables are well described by NLO QCD. Furthermore it has been demonstrated that the dependences of the internal jet structure on the E_T and η is well reproduced by QCD models [14].

The dijet cross sections $d^2\sigma/dQ^2\,d\xi$ and $d^2\sigma/dQ^2\,dx$ have been used to extract the gluon density in the proton at a factorisation scale of $\mu_f = 200\ \mathrm{GeV}^2$ which corresponds roughly to $\langle E_T^2 \rangle$. ξ is defined as $\xi = x\,(1+\hat{s}/Q^2)$, where $\sqrt{\hat{s}}$ is the invariant mass of the dijet system. For $Q^2 > 200\ \mathrm{GeV}^2$ 55% of the dijet cross section is caused by gluon induced processes. In the fit $\alpha_s(M_Z)$ is assumed to be $\alpha_s(M_Z) = 0.119 \pm 0.005$ [15]. This value has been mostly determined in processes which are independent of the proton structure. Inclusive DIS cross section at $200 < Q^2 < 650\ \mathrm{GeV}^2$ are simultaneously fitted. These data strongly constrain the quark densities, but depend only weakly on the gluon density. The resulting gluon density together with its error band is shown in Fig. 7 in the range $0.01 < x < 0.1$. The error band is dominated by the uncertainty on α_s, by the renormalisation scale dependence

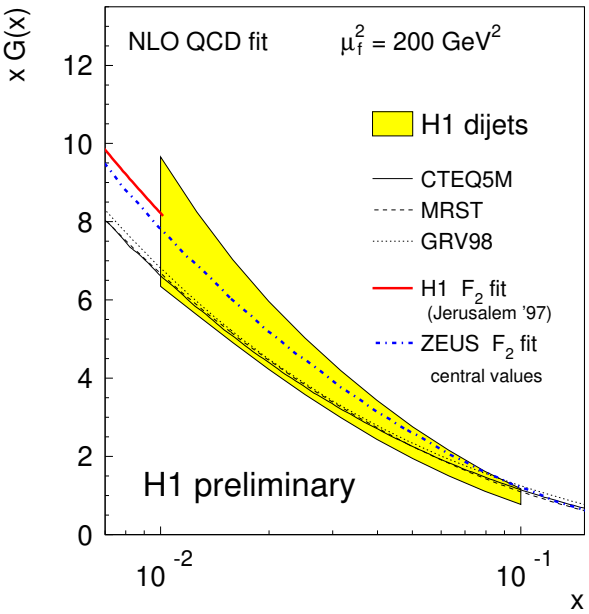

Figure 7. *The gluon density in the proton as a function of x determined in a NLO pQCD fit to dijet cross sections.*

and by the experimental absolute hadronic energy scale. Good agreement with indirect determinations via scaling violations of F_2 is found, but larger x-values are reached. Gluon determinations from global fits [16–18] tend to give slightly lower values, but are consistent within the errors.

The precise knowledge of the gluon density at large x and of α_s is an important ingredient to predict cross sections at the LHC [19]. The region $10^{-3} < x < 10^{-1}$ is directly relevant for a Higgs with mass $100 - 500$ GeV produced at $|\eta| < 2$. For instance, the cross section for the process $gg \rightarrow$ Higgs gives within 20% different results when different PDF parameterisations are used. Q^2 has to be extrapolated by DGLAP by 3 orders of magnitudes from the HERA region to reach values relevant at LHC. Therefore the precise knowledge of the parton evolution is also a key ingredient in the cross section prediction. Also the cross section $gg \rightarrow W$ which can be used as a luminosity monitor in proton-proton collisions varies within 5% when the most recent PDF of MRS and CTEQ are used. However, it is clear that comparing different PDF parameterisation is rather inadequate to estimate their uncertainty, since similar data are used in the fit and similar assumptions are made. Therefore, it is also important to develop techniques to extract QCD parameters together with an error estimate. Within one experiment H1 has demonstrated that this is perfectly possible and more results are expected in the future.

6. The Structure of the Real Photon

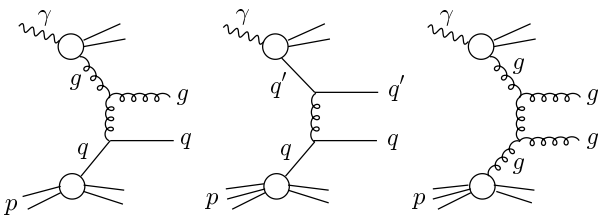

Figure 8. *Feynman diagram for resolved processes in dijet production at HERA.*

In the quark parton model DIS is viewed as a highly virtual photon interacting with partons freely moving in the proton. This is a good approximation when small distances are probed, i.e. in the limit where Q^2 is large. In this regime, the photon behaves like a point-like object, i.e. it directly couples to quarks to produce the hard scattering. At low virtualities the photon dominantly fluctuates into vector mesons. However, the photon may also fluctuate into a $q\bar{q}$ state with higher transverse energy without forming a bound state. In this case the photon acts as a source of strongly interacting partons. Such a 'resolved' process can be calculated within pQCD using the concept of a photon structure function.

They can be experimentally investigated by demanding jets or charged particles at high transverse energy in the final state. Such data are sensitiv to the quark and to the gluon content in the photon. Of particular interest is the behaviour of the photon at low fractional energies of the parton participating in the hard scattering (x_γ).

The access to low x_γ is experimenally difficult. Since x_γ is given by $x_\gamma = \sum_{1,2} E_T \; e^{-\eta}/2 \; E_\gamma$, low jet E_T destroying a good correlation with the hard partons or large η values limited by the detector acceptance and the understanding of soft

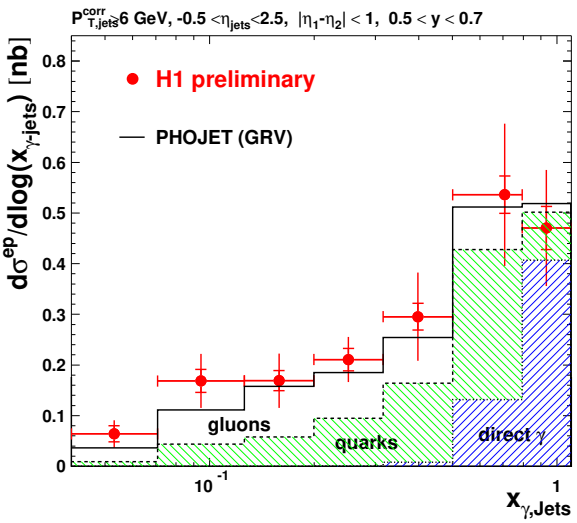

Figure 9. *Dijet cross section as a function of* x_γ.

underlying processes have to be used. In a recent analysis of photoproduced events ($Q^2 \approx 0$ GeV^2) jets are selected using a cone algorithm [20] with $R = 0.7$. After correction for energy steming from soft processes migrating into the jet cone ("pedestal") $E_T > 6$ GeV is required. Both jets have to lie well within the detector acceptance of $-0.5 < \eta_{jet} < 2.5$ and their rapidity difference must not exceed $|\Delta\eta| < 1$. The dijet cross section is shown as a function of x_γ in Fig. 9. It is compared to the LO prediction of the PHOJET [21,22] QCD model using the GRV-LO PDF [23] for the photon and the proton. While at $x_\gamma \approx 1$ the direct contribution dominates, for $x_\gamma < 1$ the resolved contribution is most important. At the lowest x_γ values gluon initiated processes are mainly responsible for the measured cross section.

A leading order interpretation of the data can be made by using the concept of an effective PDF for which the dijet cross section can be written as [24]:

$$\frac{f^{\gamma/e}(y,Q^2)}{y} \cdot \sum_{i,j}^{N_f} \frac{f^{i/\gamma}_{\rm eff}(x_\gamma, E_T^2, Q^2)}{x_\gamma} \cdot \frac{f^{j/p}_{\rm eff}}{x} \cdot |ME_{ij}|^2$$

where the sum runs over all scattering matrix elements depending on the scattering $\cos\theta^*$ of the processes shown in Fig. 9 folded by the density of parton j in the proton and parton i in the photon. The effective probability to find parton i in the photon can be written as:

$$f^{i/\gamma}_{eff} = \sum^{N_f}(q+\bar{q}) + \frac{9}{4}g.$$

The unfolded effective gluon distribution is shown in Fig. 10 as a function of x_γ. The gluon density rises as x_γ decreases. This rise is less pronounced than predicted by the LAC1 structure function [25], but is in agreement with the GRV expectation [23]. The results improve a previous measurement [26]. and agree with earlier results using the complementary approach of single charged particles [27].

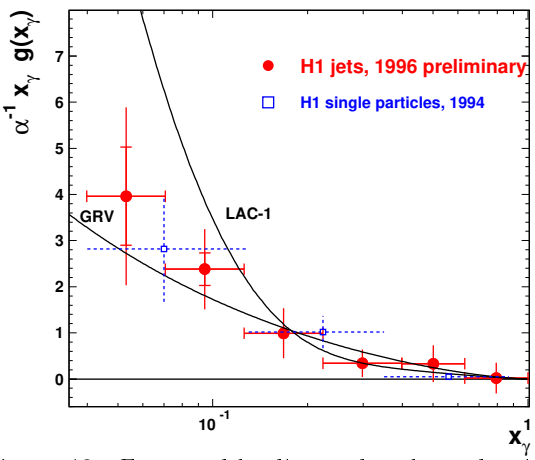

Figure 10. *Extracted leading order gluon density in the photon as a function of* x_γ.

7. Event Shapes in Current Region of Breit Frame

Measurements of event shape variables F provide information about perturbative and non-perturbative aspects of QCD. They allow to fit analytical expressions to data without referring to a fragmentation model by exploiting their characteristic power behaviour. Event shapes have been extensively studied in e^+e^-experiments at different center of mass energies [28].

Results from e^+e^-can be compared to DIS in the current hemisphere of the Breit frame. Thanks to the large kinematic range covered at HERA, the dependence of mean event shape values on a hard scale can be studied in one experiment. Event shapes like thrust, jet broadening and the jet mass have been investigated in the

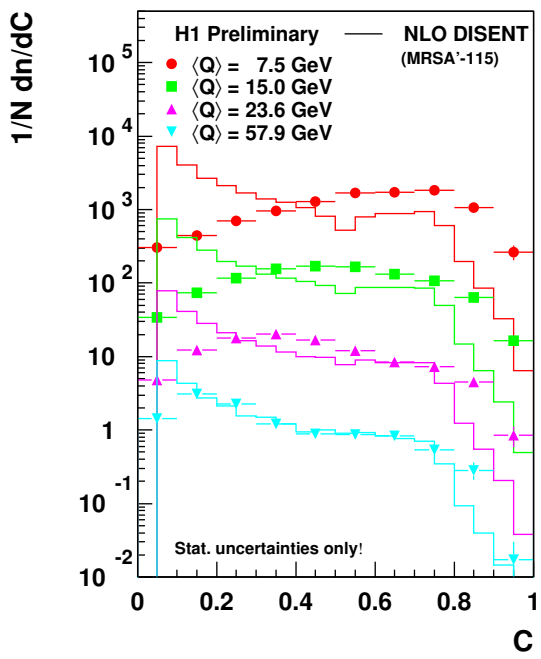

Figure 11. *Distribution of the C-parameter for various $Q = \sqrt{Q^2}$ bins.*

past [29]. In this workshop for the first time also the C-parameter and differential jet rates y_2 for the JADE and for the K_T jet algorithm have been presented.The C-parameter is defined as: $C := 3(\lambda_1\lambda_2 + \lambda_2\lambda_3 + \lambda_3\lambda_1)$ where the λ_i are the eigen values of the linearized momentum tensor of the final state particles. As an example, the distribution of the C-parameter in bins of the momentum transfer $Q = \sqrt{Q^2}$ ranging from 7 to 100 GeV is shown in Fig. 11. While at high Q the data are described by a $\mathcal{O}(\alpha_s^2)$ calculation [30], at low Q the shape does not agree with perturbative QCD. The same conclusions hold for the mean value of the C-parameter shown as a function of Q in Fig. 12.

The mean event shapes can be expressed by a perturbative and a non-perturbative contribution of the form [31,32]:

$$\langle F \rangle = \langle F \rangle^{\mathrm{pert}} + \langle F \rangle^{\mathrm{pow}}$$

$$\langle F \rangle^{\mathrm{pert}} = c_{1,F}(x)\,\alpha_s(Q) + c_{2,F}(x)\,{\alpha_s}^2(Q)$$

$$\langle F \rangle^{\mathrm{pow}} = a_F \frac{16}{3\pi}\frac{\mu_i}{Q}\ln^p\frac{Q}{Q_0}\,\left[\overline{\alpha}_0(\mu_i) - \alpha_s(Q) - \left(b\ln\frac{Q^2}{\mu_i^2} + k + 2b\right)\alpha_s^2(Q)\right]$$

where $b = (11\,C_A - 2f)/12\pi$ and $k = \left[(67 - 3\pi^2)\,C_A - 10\,f\right]/36\pi$ and $\overline{\alpha}_0$ is a free, but 'universal', effective coupling parameter below an 'infra-red' matching scale $\Lambda_{QCD} \ll \mu_i \ll Q$.

Such an ansatz is able to describe the data (see Fig. 12). The power corrections are large at low Q, but become less important with increasing Q. The parameters α_s and $\overline{\alpha}_0$ can be simultaneously fitted to the data. It turns out that the analytical form of the power correction is adequate to describe the data for all studied event shapes. A simple form $\langle F \rangle^{\mathrm{pow}} \sim 1/Q$ is not able to describe the data.

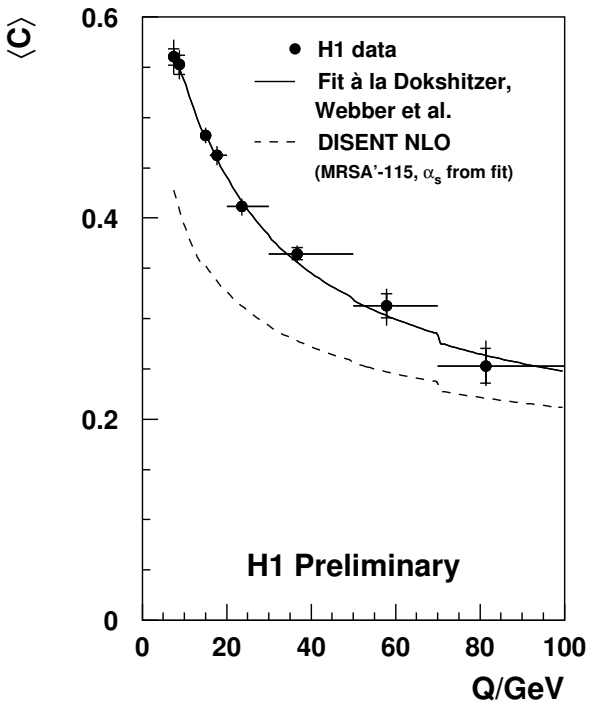

Figure 12. *Mean value of the C-parameter as a function of $Q = \sqrt{Q^2}$.*

The question whether consistent fit results are obtained when using different event shape variables is addressed in Fig. 13. The ellipse displays the 1σ and 2σ contours of the statistical and the systematical error. The NLO dependence on the renormalisation scale is not included. The experimental errors are highly correlated. The two parameters $\overline{\alpha}_0(\mu_I)$ and $\alpha_s(M_Z)$ come out about in the same range like found in e^+e^-collisions. However, in particular the large spread of α_s

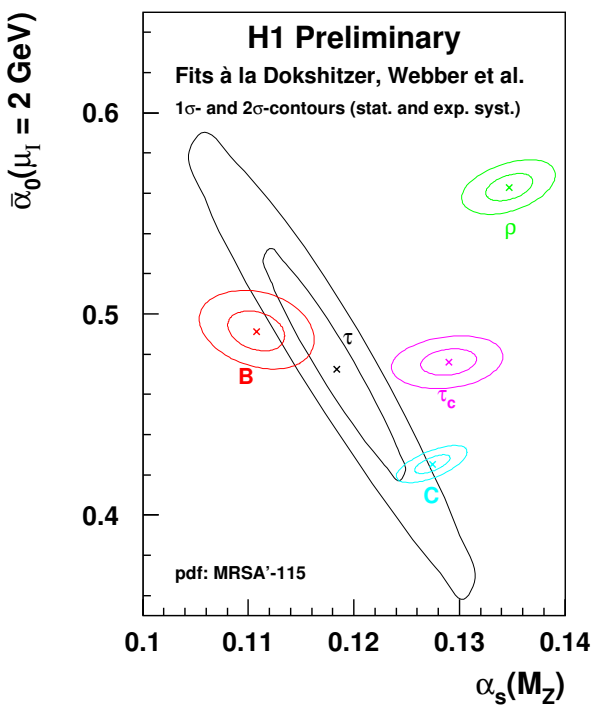

Figure 13. *$\alpha_s(M_Z)$ versus $\overline{\alpha}_0(\mu_I)$ from the fit of four different event shapes variables. The ellipse gives the 1σ and 2σ contour of the statistical and the systematical error.*

is not fully satisfactory. More precise data and more theoretical work is needed to continue this promising way to get an (analytical) understanding of hadronisation for specific variables. Open questions are the correct inclusion of higher orders to get a more consistent picture and the treatment of the uncertainty introduced by the parton density function to the fit result.

8. QCD parton dynamics at low x

At low x the simple picture of DIS as a process where a virtual photon interacts instantaneously with a point-like parton freely moving in the proton has to be modified. The phase space for gluon emission ($W^2 \approx Q^2/x$) between the photon and the proton becomes so large that many partons can be radiated before interacting with the photon. Such an interaction is illustrated in Fig. 14. In particular in the central rapidity region the

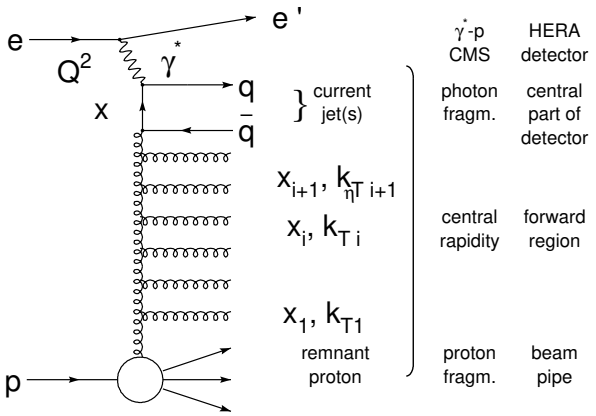

Figure 14. *Diagram of a DIS events at low x.*

detection of hard particles can discriminate between different evolution schemes of the parton cascade [33].

The transitions $g \to gg$ and $g \to q\bar{q}$ at each point in the ladder can be approximated by the DGLAP equations [34]. By resumming the $(\alpha_s \ln Q^2)^n$ terms they predict the Q^2 evolution of a parton known to be point-like at some given scale Q_0^2 to the region where the interaction with the photon takes place. To derive the DGLAP equations a strongly ordered configuration in the parton virtualities along the ladder has to be assumed. This leads to a suppression of the available phase space for gluon radiation towards the proton.

When the $(\alpha_s \ln 1/x)^n$ terms become large, they have to be taken into account, e.g. by the resummation accomplished by the BFKL equations [35]. In a physical gauge, these terms correspond to an n-rung ladder diagram in which gluon emissions are ordered in longitudinal momentum. The strong ordering of the transverse momenta is replaced by a diffusion pattern as one proceeds along the gluon chain. The BFKL equations describe how a parton in the proton is dressed by a cloud of gluons at low x localised in a fixed transverse spatial region of the proton.

The density of hard partons in the central rapidity region can be experimentally explored by identified particles or jets in the forward region of the H1 detector (see Fig. 14). The finely granulated H1 LAr calorimeter with its

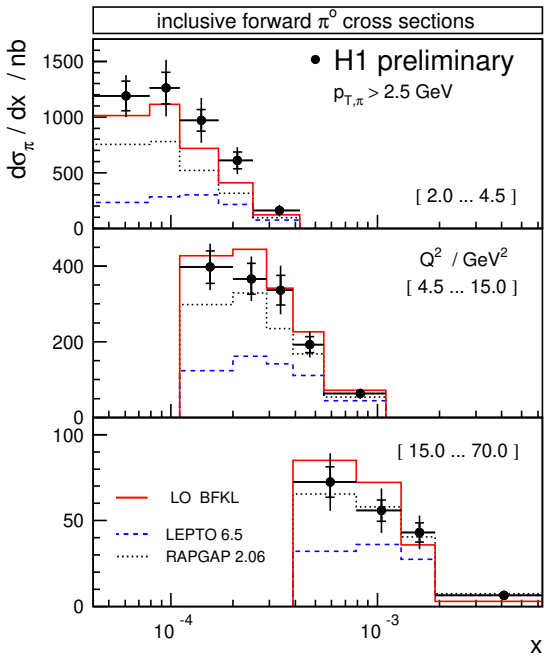

Figure 15. π^0 *cross section as a function of* x.

3.5×3.5 cm calorimeter cells and a 4 fold segmentation offers the opportunity to identify high energetic π^0 mesons by exploiting the typical properties of electromagnetic showers. The high particle density in the forward region for $5^o < \theta_{lab} < 25^o$ requires a good understanding of the detector and is the main experimental challenge. The inclusive cross section as a function of x for π^0 mesons with a $P_T^\star > 2.5$ GeV and $x_\pi = E_\pi/E_p > 0.01$ in the centre of mass system for three Q^2 regions ranging from $2.0 < Q^2 < 70$ GeV^2 is shown in Fig. 15. The cross section rises by a factor 8 towards low x for each Q^2. In the lowest Q^2 region values down to $x = 5 \cdot 10^{-5}$ are reached. A weak dependence of the cross section on Q^2 is found and for each Q^2 the x spectrum is similar. A Monte Carlo study indicates that a π^0 with $P_T^\star \approx 2$ GeV originates on average from a parton with $P_T^\star \approx 5$ GeV.

The LEPTO Monte Carlo [36] model based on the leading order matrix element ($\mathcal{O}(\alpha_s)$) $eq \to eqg$ or $eg \to eq\bar{q}$ incorporating higher order emissions from the proton side in a leading logarithm approximation close to the DGLAP equations is not able to describe the data. In the highest Q^2 bin LEPTO is below the data by a factor of 2. This difference increases towards lower Q^2. The RAPGAP model [36] includes in addition LO resolved photon processes. It is in much better agreement with the data. However, at the lowest x and Q^2 also this model fails to describe the data. An analytical calculation based on the leading order BFKL equation [37] agrees with the data. In this calculation the parton calculation is related to the measurement using a fragmentation function.

Whether this measurement can be taken as a proof that BFKL effects are needed to describe HERA data remains an open question. It is not fully transparent what approximations have been included in the calculations in view of the large NLO correction to the BFKL equation.Moreover it is not a priori clear if the fragmentation functions are valid in the high particle density environment at HERA. Furthermore, it has been shown that very similar measurements of jets in the forward region [38,39] can be described by a $\mathcal{O}(\alpha_s^2)$ calculation of direct and resolved processes [40]. Since the photon splitting term is the dominant contribution of the resolved part, this calculation suggest that a $\mathcal{O}(\alpha_s^3)$ direct calculation would be enough to describe the hadronic final state data at low x. In this case the parton ladder is not long enough such that resummation effects to all order of the $\ln(1/x)$ terms are needed in the HERA regime.

The strong rise of the inclusive π^0 cross section reminds the rise of F_2 towards low x which has been before the advent of HERA predicted by the BFKL equations. We know today that F_2 can be well described by the NLO DGLAPequations, but is also compatible with BFKL.It is interesting to note that the ratio of the forward π^0 cross section to the inclusive cross section is constant over the full x range. At $2 < Q^2 < 4.5$ GeV^2 approximately 0.2% of the DIS events contain a forward π^0 with $P_T^\star > 2.5$ GeV. At $15 < Q^2 < 70$ GeV^2 this ratio rises to 0.5%. While for an inclusive measurement the DGLAP evolution is adequate, for observables where the parton evolution is probed at a specific η region the implementation of the DGLAP equation in Monte Carlo

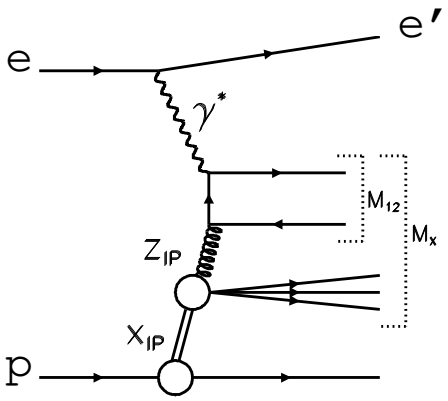

Figure 16. *Diagram for a colourless exchange in DIS.*

models are too restrictive. Only models allowing for a large phase space of parton emission are in agreement with the data.

The constant (with respect to the inclusive cross section) probability to emit hard particles in the forward region can be juxtaposed to the probability to emit no particle at all. It is known since 1993 that the ratio of events exhibiting a large rapidity gap is approximately 10% for $5 \leq Q^2 \leq 50$ GeV^2 and $2 \cdot 10^{-4} \leq x \leq 2 \cdot 10^{-2}$. Does this mean that there is a connection between the production mechanism of rapidity gap events and the parton dynamics at low x?

9. Diffraction

A new era in understanding hadronic interactions was opened by the observation that a surprisingly large fraction of DIS events ($\approx$ 10%) exhibited a rapidity region free of hadronic activity between the particles emerged from the hard scattering and the proton. Since in normal DIS large rapidity gaps are exponentially suppressed, these events were soon analysed in terms of an exchange of a colourless object probed by the virtual photon. If no quantum numbers are exchanged such interactions are called "diffractive" and the colourless object is called "pomeron" ($\mathbb{P}$)

The diagram for the production of diffractive events is depicted in Fig. 16. The hadronic final state can be split up in two distinct systems X and Y which are separated by the largest rapidity gap in the event. Usually events are selected by requiring an absence of activity in the forward part of the detector such that Y has a small invariant mass ($M_Y \lesssim 1.6$ GeV) and the squared momentum transfer t between the incoming proton and Y is small ($|t| \lesssim 1$ GeV^2). The following kinematic variables can be defined to describe the diffractive production mechanism:

$$\beta \simeq \frac{Q^2}{Q^2 + M_X^2}, \; x_{\mathbb{P}} \simeq \frac{Q^2 + M_X^2}{Q^2 + W^2}, \; z_{\mathbb{P}} \simeq \frac{Q^2 + M_{12}^2}{Q^2 + M_X^2}$$

$x_{\mathbb{P}}$ measures the fraction of the proton momentum transfered to the $\mathbb{P}$ and β is the momentum fraction of the $\mathbb{P}$ momentum carried by the quark coupling to the virtual photon. If the system M_X is further resolved in a subsystem M_{12}, the variable $z_{\mathbb{P}}$ gives the momentum fraction of the struck parton. If $M_{12}^2 < M_X^2$, i.e. $z_{\mathbb{P}} < 1$, not the entire energy from the colourless exchange takes part in the hard scattering.

Usually the diffractive interaction is described in terms of Regge phenomenology and the kinematic dependences are parameterised as:

$$\frac{d\sigma}{dt dM_X^2} \propto \left(W^2\right)^{2\alpha_{\mathbb{P}}(t)-2} e^{b_0 t}$$

where $\alpha_{\mathbb{P}}(t)$ is the effective leading Regge trajectory. For soft diffractive processes, $\alpha_{\mathbb{P}}(t)$ takes the universal form $\alpha_{\mathbb{P}}(t) \sim 1.08 + 0.2\, t$. When a hard scale is present, $\alpha_{\mathbb{P}}(0)$ (t-slope) is expected to increase (decrease).

The "soft" pomeron ansatz successfully describes the total and elastic hadron-hadron and hadron-photon cross section as well as the energy dependence of the cross section of light vector mesons ($M_X = M_V$). However, a single soft pomeron does not describe all diffractive data measured at HERA. In presence of a hard scale like Q^2 or a larger vector meson mass the cross section steeply increases with $W_{\gamma p}$. A new type of dynamical pomeron may begin to play a role whose structure can be tested in DIS. HERA allows diffractive interactions to be analysed in terms of parton dynamics and offers the possibility to study the transition between perturbatively calculable and incalculable strong interactions.

9.1. Inclusive Diffractive measurements

The inclusive diffractive data are consistent with a partonic interpretation of the pomeron for which the cross section factorises into the parton density of the pomeron and a pomeron flux factor describing the probability to find a pomeron in the proton [41]. The parton densities can be determined by a QCD analysis [42] of the inclusive diffractive cross section:

$$\frac{d^3\sigma_{ep\to eXY}}{dQ^2 d\beta dx_{I\!P}} = \frac{4\pi\alpha^2}{\beta Q^4}(1-y+\frac{y^2}{2})F_2^{D(3)}(x_{I\!P}, Q^2, \beta).$$

At fixed $x_{I\!P}$ the Q^2 dependence of the diffractive structure function $F_2^{D(3)}(x_{I\!P}, Q^2, \beta)$ is rather flat. The β dependence exhibits a logarithmic rise characteristic for scaling violations. When fixing the quark and gluon distribution at a starting scale of $Q_0^2 = 3\ \mathrm{GeV}^2$ and evolving them to larger Q^2 using the DGLAP equations, it is found that most of the partonic content of the pomeron is carried by hard gluons. At $Q^2 = 4.5$ GeV^2 the pomeron consist to 90% of gluon and even at $Q^2 = 75$ GeV^2 the gluon fraction is still 80%. Using these fits performed for $Q^2 < 100$ GeV^2 also the new H1 data reaching Q^2 up to 800 GeV^2 can be described. However, in an analysis of very low Q^2 data ranging down to 1 GeV^2 the logarithmic β dependence flattens off around $Q^2 \approx 3-4$ GeV^2.

9.2. Diffractive Dijet Production

The partonic structure of diffractive interactions can be further tested in the hadronic final state. High transverse momentum jet production is directly sensitive to the gluon content. For $7.5 < Q^2 < 80$ GeV^2 and $0.1 < y < 0.7$ exactly two jets are selected with $E_{T,jet} > 5$ GeV. Jets are defined by the cone algorithm. $E_{T,jet}$ is measured relative to γ^* axis in rest frame of the system X. The dijet cross section as a function of $z_{I\!P}$ is shown in Fig. 17. Models in which the pomeron is dominated by gluons (fit 1 and 2 in [42]) describe the data well. Models where the pomeron consist only of quarks at the starting scale undershoot the data by a factor of 5.

An alternative model sees the diffractive interaction as $q\bar{q}$ fluctuation of the photon (decomposed in Fock states) coupling via two gluons to the proton [43,44] in a colour singlet configuration (2-gluon model). At the largest $z_{I\!P}$ values, where the full momentum of the X system is carried by the two jets and the model is expected to be valid, it is somewhat below the data, but still compatible with them given the large systematic error.

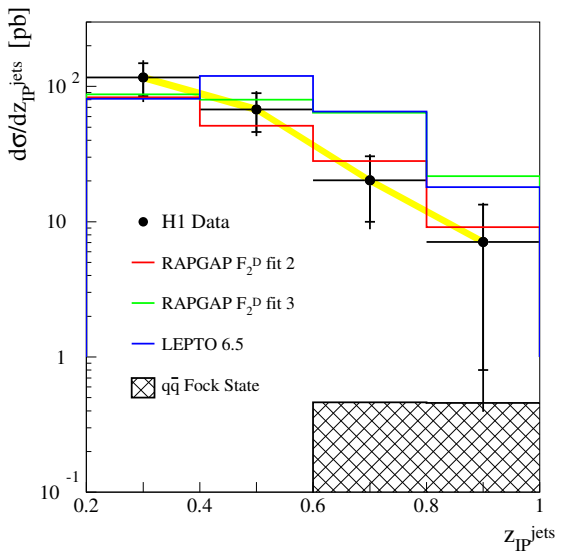

Figure 17. *Diffractive jet cross section as a function of* $z_{I\!P}$.

In conclusion, dijet data support the gluon dominated partonic picture of the pomeron.

10. Diffractive Charm Production

The rôle of gluons in the diffractive production mechanism can be directly assessed by tagging charmed quarks in the hadronic final state, since they predominately originate from Boson-gluon processes. Charm quarks are identified by reconstructing $D^{*\pm}$ mesons in the classical decay chain $D^* \to D^0\pi^+_{slow} \to (K^-\pi^+)\pi^+_{slow}$. The branching ratio of this process is only 2.6%. In the kinematical region of $2 < Q^2 < 100$ GeV^2 and $0.05 < y < 0.7$ 45 events have been selected in a data sample of about 21 pb^{-1} taken in $1995-1997$. D^* mesons were required to have $p_T > 2$ GeV and $|\eta| < 1.5$. The total cross section is measured to be:

$$\sigma_{vis}(ep \to (D^*X)Y) = 154 \pm 40(stat) \pm 35(syst)\,\mathrm{pb}.$$

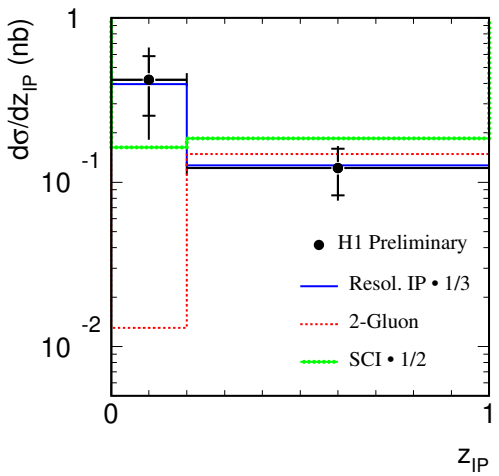

Figure 18. *Diffractive charm cross section as a function of* $z_{\mathbb{P}}$. *The pomeron model has been divided by a factor of* 3, *the soft colour model by a factor of* 2.

In Fig. 18 the visible cross section $\sigma_{vis}(ep \to (D^*X)Y)$ is shown as a function of $z_{\mathbb{P}}$. As for the diffractive jet data the cross section rises towards low $z_{\mathbb{P}}$. This means that in most of the events a part of the hadronic final state produced in the diffractive exchange is not associated with the hard subprocess.

The shape of the $z_{\mathbb{P}}$ distribution is well reproduced by the gluon dominated partonic pomeron picture. This model remarkably reproduces the rise of the cross section towards low $z_{\mathbb{P}}$. However, the normalisation is off by a factor of 3 ! Hence, much less charm quarks are produced in the hadronic final state than predicted by the parton density function extracted from the inclusive diffractive measurements and applied to the pomeron picture.

In the region where the hadronic system X dominantly consists of the $c\bar{c}$ pair alone (i.e. $z_{\mathbb{P}} \approx 1$) the 2-gluon model gives a fair description of the data. As in the case of the diffractive dijets it is not able to describe the the low $z_{\mathbb{P}}$ region. The soft colour interaction model where the colour structure of a normal DIS events is modified by a soft interaction leading to a colour singlet in the final state [45] can not describe the overall normalisation nor the shape of the $z_{\mathbb{P}}$ distribution.

In conclusion, the diffractive charm signal is more pronounced at low $z_{\mathbb{P}}$ values. The data therefore indicate that not the entire colourless exchange couples to $c\bar{c}$ system. The behaviour is well reproduced by the "pomeron" model, but the overall measured cross section is three times lower than expected. This is the first time that this picture which has been so far supported by all inclusive and hadronic final state data is put into question. More data are needed to clarify the situation.

11. Vector Mesons

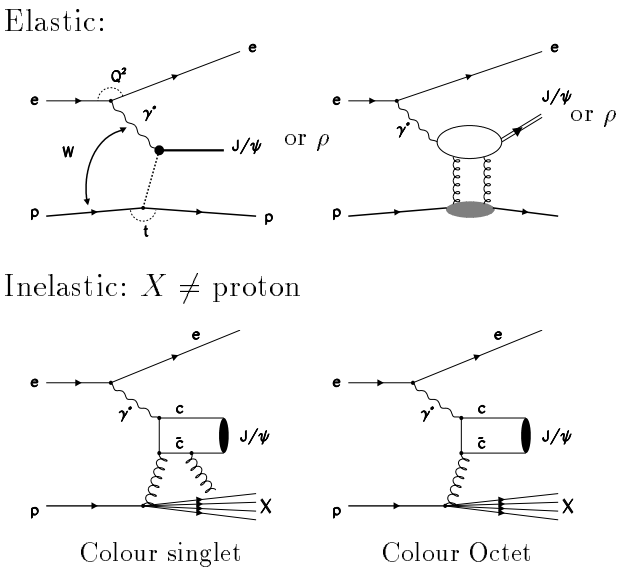

Figure 19. *Diagram for vector meson production.*

HERA allows to study the simplest photon-hadron diffractive reaction $\gamma^* p \to$ VM p in a new range of $\gamma^* p$ centre of mass energies up to $W_{\gamma p} \lesssim 300$ GeV. It is possible to investigate the transition from the soft regime of photoproduction of light vector mesons at low momentum transfers to the pQCD regime in the presence of three hard scales: Q^2, $M_X = M_V$ and t. The traditional way of modelling vector meson production is the vector meson dominance model where the photon fluctuates into a vector meson which then elastically scatters off the proton. In such a picture only a weak energy dependence of the cross section is expected [46] (see Fig. 19 upper left). This works well for light vector mesons at

low Q^2 and t. For heavier vector meson like the J/ψ the charm mass provides a hard scale and pQCD calculations are possible. An example for such a pQCD model where the J/ψ couples via two gluons to the proton is shown in Fig. 19 (upper right).

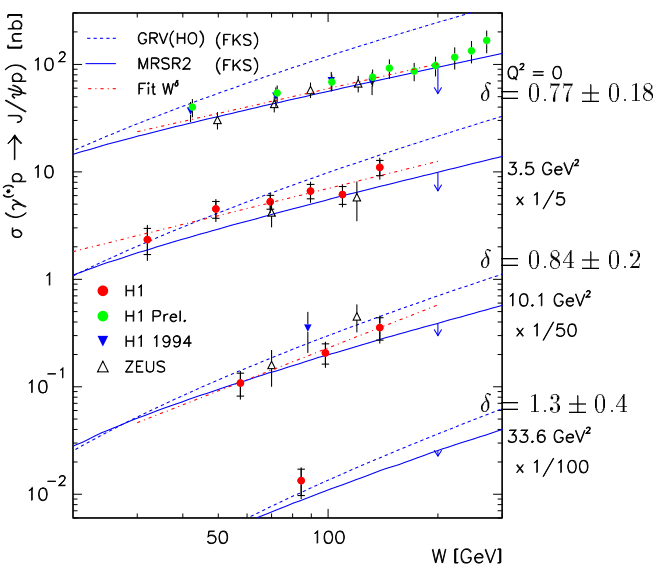

Figure 20. *The elastic J/ψ cross section as a function of $W_{\gamma p}$.*

The measured elastic J/ψ cross section as a function of $W_{\gamma p}$ is displayed in Fig. 20 for $0 < Q^2 < 33$ GeV^2. A wide $W_{\gamma p}$ range from $50 < W_{\gamma p} < 285$ GeV is covered. A much steeper rise ($W_{\gamma p}^{0.77\pm0.18}$) than predicted by soft models ($W_{\gamma p}^{0.32}$) is observed in the data. However, the data are well described by a QCD inspired calculation [47]. The arrow indicates the uncertainty introduced by the charm mass ($m_c = 1.4 - 1.5$ GeV). Since the gluon density enters squared in the calculation this measurement is sensitive to the gluon distribution in the proton. The cross section decreases as $1/(Q^2 + M^2_{J/\psi})^n$, where $n = 2.38 \pm 0.11$, as Q^2 increases. The data are not precise enough to see a further steepening of the rise with increasing Q^2. In conclusion, VDM holds unless there is a hard scale in the problem. The failure of this picture together with the sucess of QCD inspired models gives additional confidence in the potential of QCD to describe processes where the scales involved are surprisingly small. Further studies will gain a better understanding of the transition from the region governed by soft interactions to the regime where pQCD turns on.

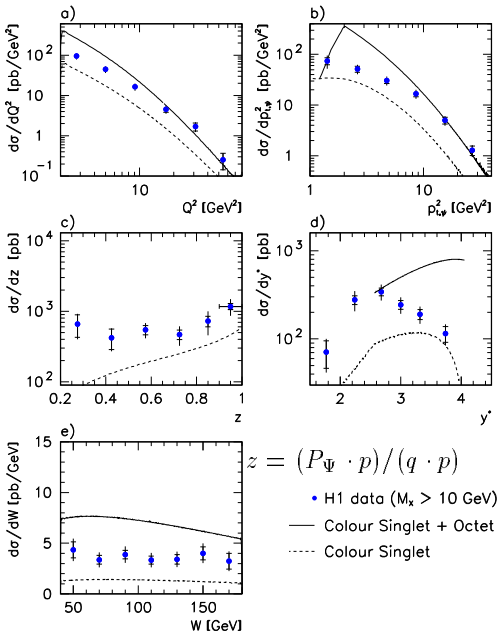

Figure 21. *Differential cross section for inelastic J/ψ production as a function of Q^2, P_T^2, z, $W_{\gamma p}$ and the rapidity.*

Inelastic vector meson production is characterised by an inelasticity $0 < z = (P_\Psi \cdot p)/(q \cdot p) < 0.9$ and a relatively large mass M_X. Two models for the production meachnism are shown in the lower part of Fig. 19. In a short distance process a $c\bar{c}$ state is produced in a boson-gluon fusion. The $c\bar{c}$ system is therefore a colour octet. The long range transition into the J/ψ has therefore to involve the emission of an additional gluon. The failure of this approach to describe the production of quarkonia at large P_T, in particular at TEVATRON, led to the inclusion of additional contributions where the $c\bar{c}$ system transforms into an colour singlet in a long range interaction without emitting a gluon [48]. The long range matrix elements have been fitted to the $p\bar{p}$ data. It is therefore interesting to see, if these fits can be sucessfully applied to HERA data.

The differential cross section for inelastic J/ψ production defined by $M_X > 10$ GeV is

shown in Fig. 21. The colour octet model is overlayed as dashed the singlet model as solid line. Both predictions [49] fail to describe the shape of the data. The colour singlet is a factor $2-3$ below the data, the sum of the singlet and octet model is too large. The reason for this failure is unknown. It seems that an overall adjustment of transition matrix element is necessary. The failure to describe the shape also calls for an relative adjustment of individudal contributions. Recently it has been reported that the inclusion of higher order radiation (in a Monte Carlo approach) lowers the colour octet matrix elements needed to describe the TEVATRON data [50]. Similar effects might also be important at HERA.

12. Conclusions

In the past years HERA has been operated very successfully and provided useful $e^{\pm}p$ data sets. From the recent 1998/1999 $e^{-}p$ running period neutral and charged current DIS cross section have been measured. The observed difference in the $e^{-}p$ and $e^{+}p$ data provides clear evidence for electroweak interference effects. HERA starts to probe the electroweak sector of the Standard Model. So far, no striking deviations have been seen, although for $Q^2 > 15000$ GeV^2 more events than expected are found in the $e^{+}p$ data. Future high precision data will reveal, if this is only a statistical fluctuation or if it is a first hint for a new interaction on top of QCD. The HERA collider will be upgraded in the year 2000 to deliver an integrated luminosity of 150 pb^{-1} per year. This will allow to accumulate $\int \mathcal{L}dt \approx 1$ fb^{-1} until the year 2006.

Precise data on the proton structure function constrain the parton density functions in the proton. This inclusive measurement is consistent with the parton evolution according to the DGLAP equations. The gluon density has been directly measured from observables based on the hadronic final state like dijet and charm production. One of the biggest uncertainties in these measurement is the unknown relation between the partonic final state and the measurable hadrons. First steps to develop analytical calculations for specific observables based on the hadronic final state in the current hemisphere of the Breit system are very encouraging. Further theoretical and experimental work is needed here.

New tests of forward particle production put the DGLAP evolution scheme into question. More partonic activity seems to be required. Moreover it has been observed that the probability to emit hard partons in the forward region is constant with respect to the inclusive cross section. This is very similar to the behaviour of event where no particles are emitted in a rapidity region.

So far HERA data have supported a consistent picture of the production mechanism of rapidity gap events. New results on diffractive charm production seem to be in disagreement with the pomeron picture. More data are needed to clarify this situation.

Precise data on vector meson production are now available. In the elastic channel QCD models are able to describe the data. However, in the inelastic channel no satisfying calculation is available.

Acknowledgments

I would like to thank the organisers for this stimulating workshop. It is a pleasure to thank my colleagues from the H1 collaboration for their enthusiasm to produce the results which made this report possible. Many to thanks to M. Erdmann for the critical reading of the manuscript.

REFERENCES

1. W. Buchmüller, R. Rückl and D. Wyler, *Phys. Lett. B 191* (1987) 442.
2. H1 Collab., In *Conf. paper 579, XXIX ICHEP* (1998).
3. U. Baur, J.A.M Vermaseren and D. Zeppenfeld, *Nucl. Phys. B 375* (1992) 3.
4. Particle Data Group, C. Caso et al., *Eur. Phys. J. C 3* (1997) 1–794.
5. H1 Collab., S. Aid et al., *Nucl. Phys. B 470* (1996) 3.
6. H1 Collab., S. Aid et al., *Phys. Lett. B 393* (1997) 452.
7. H1 Collab., S. Adloff et al., *Nucl. Phys. B 497* (1997) 3.

8. H1 Collab., C. Adloff et al., *Phys. Lett. B 393* (1997) 452.
9. A.C. Benvenuti et al., *Phys. Lett. B 223* (1989) 485.
10. M. Arneodo et al., *Nucl. Phys. B 483* (1997) 3.
11. S. D. Ellis and D. E. Soper, *Phys. Rev. D 48* (1993) 3160.
12. S. Catani, Yu. L. Dokshitzer, M.H. Seymour and B.R. Webber, *Nucl. Phys. B 406* (1993) 347–353.
13. S. Catani, Yu.L. Dokshitzer and B.R. Webber, *Phys. Lett. 285* (1992) 291–299.
14. H1 Collab., C. Adloff et al., *Nucl. Phys. B 545* (1999) 3.
15. S. Catani, In *XVIII Int. Symp. on Lepton Photon Interactions* (1997), Hamburg (Germany) and hep-ph/9712442.
16. A.D. Martin, R.G. Roberts, W.J. Stirling and R.S. Thorne, *Eur. Phys. J C 4* (1998) 463.
17. H.L. Lai et al., In *hep-ph/9903282* (1999).
18. M. Glück, E. Reya and A. Vogt, *Eur. Phys. J. C 5* (1998) 461.
19. J. Stirling, In *LHC theory workshop* (1998), CERN, Geneva.
20. CDF Collab., F. Abe et al., Phys. Rev. D 45 (1992) 1448–1458.
21. R. Engel, *Z. Phys. C 66* (1995) 203.
22. R. Engel and J. Ranft, *Phys. Rev. D 54* (1996) 4244.
23. M. Glück, E. Reya and A. Vogt, *Z. Phys. C 53* (1992) 127–134.
24. B. L. Combridge and C. J. Maxwell, *Nucl. Phys. B 239* (1984) 429.
25. H. Abramowics, K. Charchula and A. Levy, *Phys. Lett. B 269* (1991) 458.
26. H1 Collab., T. Ahmed et al., *Nucl. Phys. B 445* (1995) 195.
27. H1 Collab., C. Adloff et al., *subm. to Eur. Phys. J C* (1998) DESY 98–148.
28. S. Bethke, In *Int. Euroconf. on QCD* (1997), Montepellier (France) and hep-ph/9710030v2.
29. H1 Collab., C. Adloff et al., *Phys. Lett. B 406* (1997) 256.
30. S. Catani and M. Seymour, *Nucl. Phys. B 485* (1997) 291.
31. B.R. Webber, Phys. Lett. 339 (1994) 148; Yu. L. Dokshitzer and B.R. Webber, Phys. Lett. B352 (1995) 451, B404 (1997) 321; M. Dasgupta and B.R. Webber, Eur. Phys. J. C1 (1998) 539.
32. Yu. L. Dokshitzer and B. Webber, Phys. Lett. B404 (1997) 321.
33. M. Kuhlen, *Phys. Lett. B 382* (1996) 441.
34. Yu. L. Dokshitzer, Sov. Phys. JETP 46 (1977) 641; V.N. Gribov and L.N. Lipatov, Sov. J. Nucl. Phys. 15 (1972) 438 and 675; G. Altarelli and G. Parisi, Nucl. Phys. 126 (1977) 297 .
35. E.A. Kuraev, L.N. Lipatov and V.S. Fadin, Sov. Phys. JETP 45 (1972) 199; Y.Y. Balitsky and L.N. Lipatov, Sov. J. Nucl. Phys. 28 (1978) 282.
36. G. Ingelman, A. Edin and J. Rathsman, *Comp. Phys. Comm. 101* (1997) 108.
37. J. Kwiecinski, A.D. Martin and J.J. Outhwaite, *hep-ph/9903439* (1999).
38. H1 Collab., C. Adloff et al., *Nucl.Phys. B 538* (1999) 3–22.
39. ZEUS Collab., J. Breitweg et al., *Eur. Phys. J. C 6* (1999) 239–252.
40. B. Pötter and G. Kramer, *Phys. Lett. 453* (1999) 295–301.
41. G. Ingelmann and P.E. Schlein, *Phys. Lett. B 152* (1985) 256.
42. H1 Collab., C. Adloff et al., *Z.Phys. C 76* (1997) 613.
43. J. Bartels, H. Lotter and M. Wüsthoff, *Phys. Lett. B 379* (1996) 239.
44. J. Bartels, C. Ewerz, H. Lotter and M. Wüsthoff, *Phys. Lett. B 386* (1996) 389.
45. A. Edin, G. Ingelman and J. Rathsman, *Z. Phys. C 75* (1997) 57.
46. A. Donnachie and P.V. Landshoff, Z. Phys. C 61 (1994) 139.
47. L. Frankfurt, W. Koepf and M. Strikman, *Phys. Rev. D 57* (1998) 512.
48. E. Braaten and S. Fleming, *Phys. Rev. Lett. 74* (1995) 3327.
49. S. Fleming and T. Mehen, *Phys. Rev. D 57* (1998) 1846.
50. B. Cano-Coloma and M. A. Sanchis-Lozano, *Nucl. Phys. B508* (1997) 753.